Sliding Mode Based Powertrain Control for Efficiency Improvement in Series Hybrid-Electric Vehicles

Metin Gokasan, *Member, IEEE*, Seta Bogosyan, *Senior Member, IEEE*, and Douglas J. Goering

Abstract—This study involves the improvement of overall efficiency in series hybrid-electric vehicles (SHEVs) by restricting the operation of the engine to the optimal efficiency region, using a control strategy based on two chattering-free sliding mode controllers (SMCs). One of the designed SMCs performs engine speed control, while the other controls the engine/generator torque, together achieving the engine operation in the optimal efficiency region of the torque-speed curve. The control strategy is designed for application on a SHEV converted from a standard high mobility multipurpose wheeled vehicle (HMMWV) and simulated by using the Matlab-based PNGV Systems Analysis Toolkit (PSAT). The performance of the control strategy is compared with that of the original PSAT model, which utilizes PI controllers, a feedforward term for the engine torque, and comprehensive maps for the engine, generator and power converter (static only), which constitute the auxiliary power unit (APU). In this study, in spite of the simple modeling approach taken to model the APU and the optimal efficiency region, an improved performance has been achieved with the new SMC based strategy in terms of overall efficiency, engine efficiency, fuel economy, and emissions. The control strategy developed in this work is the first known application of SMC to SHEVs, and offers a simple, effective and modular approach to problems related to SHEVs.

Index Terms—Auxiliary power unit (APU), engine optimal efficiency operation, series hybrid electric vehicles (HEVs), sliding mode controller (SMC).

I. INTRODUCTION

HYBRID electric vehicles (HEVs) offer the most economically viable choices in today's automotive industry, while also providing solutions for high fuel economy and very low emissions. The most common HEVs take on two major forms; series and parallel HEVs. The drawbacks of the series HEVs (SHEVs) over parallel types are the requirement for two electrical machines and larger dimensions for the traction motor, in addition to the losses incurred during the conversion of the mechanical to electrical energy and back to mechanical energy again. On the other hand, the mechanically decoupled structure

of the engine from the wheels in SHEVs also presents some advantages; i.e., the use of electric motors alone for traction gives rise to the possibility of very low operating noise, offering benefits particularly in military operations; additionally, higher efficiency levels can be achieved for the engine by not allowing its operation outside of its optimal efficiency region, except for short transient durations. For more information on HEVs and electrical vehicles (EVs), the readers is referred to [1]–[5] addressing many important aspects of the technology involved and [6] and [7] for the modeling and control of power trains in both parallel and series type HEVs.

The SHEV powertrain considered in this work consists of a battery bank and an engine-generator set which is referred to as the auxiliary power unit (APU), two traction motors, and power electronic circuits to drive the generator and traction motors. The control unit of the powertrain executes two main control algorithms.

1) Control of the traction motors, which involves the delivery of the torque value (demanded by the driver) to the wheels.
2) Control of the APU, which is particularly important in terms of efficiency and emissions in SHEVs. The general strategy is based on the operation of the engine in its optimal efficiency region with the consideration of the battery state-of-charge (SOC). By controlling the engine speed and generator torque, the engine is forced to operate in its highest possible efficiency region.

In the existing literature related to SHEVs, studies are mostly concentrated on the control of the APU. Among these studies, [8] presents a fourth-order linear adaptive dynamic programming method for the control of the APU. This method requires minimal *a priori* knowledge of the plant. In [9], cascade PI controllers are utilized for APU control. The signal obtained with the addition of a feedforward term to the cascade PIs used for engine speed control in the outer loop, performs the torque control of the generator. However, the highly nonlinear nature of the system poses problems in the determination of PI controller parameters and feedforward terms. A simulation program called PSIM is given in [10], presenting simulation results for logic decision mechanisms designed for the control strategy of both series and parallel HEVs. [11] introduces a control rule based on complex calculation methods that make use of the engine efficiency map, driver power demand, dc source and battery model. In [12], a Matlab/Simulink based model is derived for the simulation of SHEVs and in [13], this model is used for the simulation of the system under different driving schedules. In [14], two algorithms are developed for SHEV control to achieve maximum energy efficiency by determining the generator ON/OFF period and to produce demanded torque when the generator is

M. Gokasan is with the Electrical-Electronics Engineering Facility, Istanbul Technical University, Istanbul, Turkey. He is also with the Electrical and Computer Engineering Department, University of Alaska, Fairbanks, AL 99701 USA.

S. Bogosyan is with the Electrical and Computer Engineering Department, University of Alaska, Fairbanks, AK 99775 USA (e-mail: s.bogosyan@uaf.edu).

D. J. Goering is with the Mechanical Engineering Department University of Alaska, Fairbanks, AK 99775 USA.

ON. One of the algorithms is used for the derivation of the battery SOC, maximum power and losses, while the second algorithm makes some forecasts of the system load. However, the synthesis of the two algorithms requires a number of complicated routines as well as modeling of various components, such as the battery.

Time varying parameters and the highly nonlinear nature of the vehicle systems make them very suitable for sliding mode control (SMC), which is a widely used robust control method [15], also gaining popularity in automotive applications due to its robustness against parameter and model uncertainties, as well as external disturbances. Some of the most recent literature using various SMC designs for the control of internal combustion engines in standard automotive vehicles can be listed as follows: in [16], a basic discontinuous SMC structure is employed, which is designed based on the concept of zero dynamic stability to determine and minimize the number of states in the control structure; in [17], a second-order SMC is designed and its performance is compared to that of a PI controller with experiments; in [18], several SMC design methods are presented for recent automotive applications; in [19], a SMC is proposed which involves designing an additional observer to reconstruct the system states for use by the controller and finally, in [20], a sliding mode control (SMC) based algorithm is designed for the operation of the engine in the optimal efficiency region, with the engine being operated only when SOC falls under a preset limit.

The major contribution of this study is the development of two chattering—free SMCs for the engine speed and torque control to achieve increased overall efficiency in SHEVs. To the authors' best knowledge, this is the first known application of SMC to SHEVs for the simultaneous control of the engine speed and generator torque in order to operate the engine in its optimal efficiency region. The proposed control also aims to exploit the robustness properties of SMC against the model and parameter uncertainties of the APU components; namely, the engine, generator and power converter. The control strategy is designed for application on the recent SHEV prototype, XM1124, converted from a standard high mobility multipurpose wheeled vehicle (HMMWV) and is mainly based on the operation of the engine only when necessary (i.e., when the battery SOC drops below a predetermined level), and stopping engine operation as soon as the SOC increases above that given level. The two chattering-free SMCs are run simultaneously to achieve the optimal efficiency operation of the engine; to this aim, one of the controllers maintains the engine speed in the optimum region, while the other SMC keeps the engine torque in the optimal region by controlling the power converters of the generator. The major advantage of the designed SMCs is the robustness provided against parameter and model uncertainties as well as external disturbances, which, in turn, allows simple models to be used for the engine, generator and converter. The developed control methods in this study are tested on a computer simulation model of a XM1124 prototype created using the Matlab/Simulink based PNGV System Analysis Toolkit (PSAT Version 4.1) [21], [22]. As explained in [23], the verification of the PSAT based simulated data with the actual data obtained during field testing of the prototype HMMWV has indicated that the PSAT simulation model could be used with minor modifications to provide a baseline upon which alternate components, configurations, and control strategies can be built and evaluated. However, a different and simpler control strategy is developed in this study than the one employed by the PSAT model, which offers ease of application and flexibility for actual implementation. The simulation results obtained with the two SMCs developed in this study have also yielded an improved performance in terms of engine, and overall efficiency, fuel economy, lower emissions and higher final SOC, when compared to the original PSAT results. In this study, the main aim is increasing overall efficiency by the appropriate control of the APU; hence, the control of traction motor is outside the scope and is performed using the algorithm offered by the original PSAT program.

The paper is organized as follows; after the introduction in Section I, the vehicle system is presented briefly in Section II. Next, the mathematical model of the HEV and the development of the control strategy are given in Sections III and IV, respectively. Finally, the simulation results are presented in Section V, with conclusions given in Section VI.

II. VEHICLE SYSTEM

The U.S. military has evaluated several prototype hybrid-electric versions of its HMMWV with the goals of improving fuel efficiency and range, allowing the vehicle to act as a field deployable APU, improving stealth capability, and maintaining the overall operational and transportability characteristics of the standard HMMWV (see Fig. 1). A recent prototype, the XM1124, manufactured by AM General and PEI, is a series powered hybrid with a traction motor directly coupled to each axle's differential. The standard internal combustion engine and drivetrain in the XM1124 have been replaced with an engine-generator set (APU) that provides power to the vehicle electrical bus. The bus connects all major components including the battery pack, APU, and traction motors. In this manner, the traction motors may draw power from the batteries or the APU, as determined by the control strategy.

The APU is comprised of a diesel engine coupled with an ac permanent-magnet synchronous (PMS) generator. The engine is a 2.2-l, four-cylinder, turbocharged diesel engine manufactured by Peugeot, generating 100 kW at 4000 rpm. The generator is a UQM Technologies (Model SR286) brushless motor/generator with a rated output of 100 kW and approximately 90% efficiency. The XM1124 has no transmission nor transfer case. Control of vehicle speed and braking as well as charge and discharge of the battery pack is accomplished via on-board control units.

The vehicle's battery pack consists of 24 Optima spiralcell deep-cycle batteries connected in series. These are commercially available lead-acid batteries with a nominal voltage of 12 Vdc. This results in a nominal battery pack voltage of 288 Vdc. As with all series configured HEVs, power is delivered to the loads from the battery pack which is, in turn, charged by the generator. The charge/discharge strategy for the battery pack is controlled by the XM1124s on-board controller.

The primary load consists of the two traction motors, which are also UQM SR286 brushless motor/generators. One motor is directly coupled to the rear differential while the other is coupled to the front differential via a short drive shaft to allow for off-center mounting. The rotational speed of these motors, and thus the speed of the vehicle, is controlled through a pulse-width
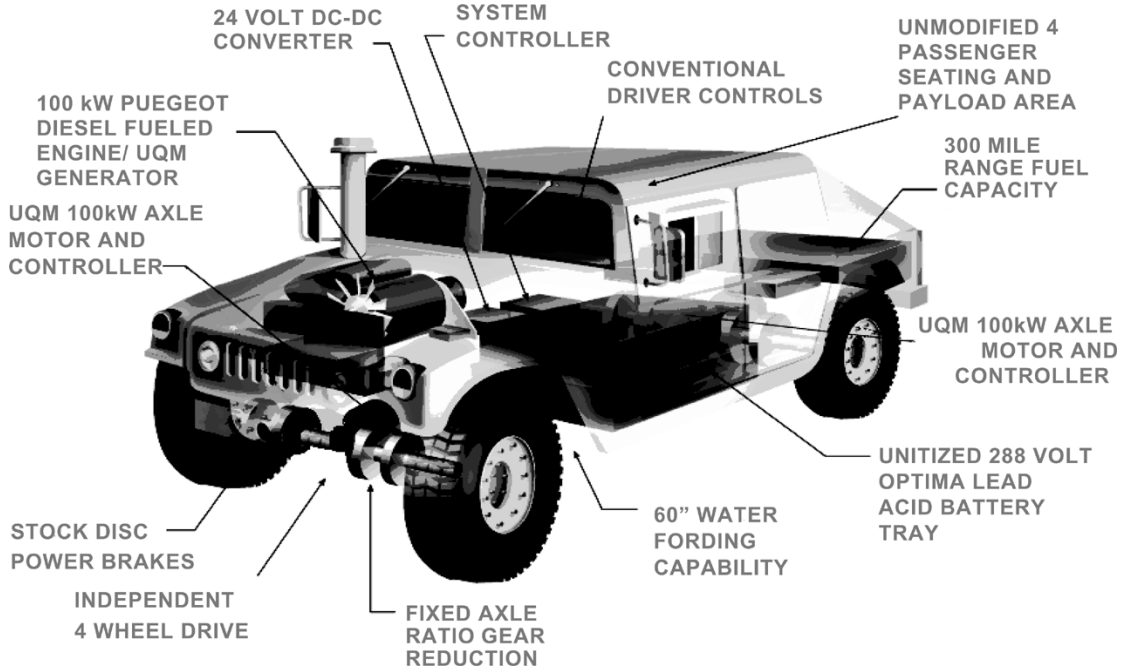
Fig. 1. Schematic diagram of HE-HMMWV.

modulation (PWM) strategy based on the position of the accelerator pedal and feedback from the speedometer circuitry.

In addition to the standard HMMWV parasitic electrical loads (e.g., lights, heater fan), the hybrid electric-HMMWV (HE-HMMWV) includes several other major electrical loads that would be driven by the engine on a standard vehicle. The standard radiator is replaced by a five-circuit cooling system. These circuits serve the engine, generator, front and rear traction motors, and the on-board controllers, respectively. The coolant circulation pump is driven by an electric motor since the diesel engine is not in continuous operation. Another electric motor powers a hydraulic pump. Hydraulics are used for the power steering and braking and also power the fans that force cooling air across the radiator. Finally, two small electric fans cycle to provide cooling for the battery pack. These parasitic electrical loads amount to 1.4–2.3 kW even when the vehicle is at rest.

III. MATHEMATICAL MODEL OF HEV

Fig. 2 demonstrates the drivetrain of the SHEV system taken into consideration in this study.

As can be seen in the diagram, the system consists of a diesel engine, a permanent magnet synchronous generator (PMSG) with its driver (ac/dc), two traction motors with their drivers (dc/ac), a bidirectional dc–dc converter and a group of batteries. The engine, PMSG and its driver are known as the APU. The APU and battery provide a dc bus which supplies two traction motor drivers (dc/ac). In this system, the generator is capable of working as an alternator or a starter (to deliver engine starting torque). The motors and generator are driven by insulated gate bipolar transistor (IGBT) converters.

To develop the control algorithms for the APU system, first the modeling of the engine and the generator will be performed.
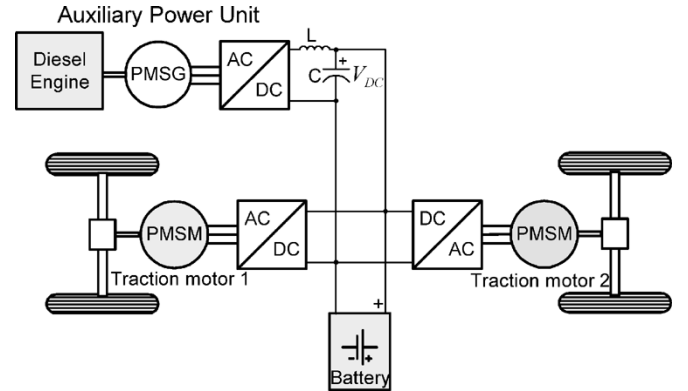

Fig. 2. Schematic diagram of series HEV drivetrain.

A. Modeling of the Engine

The modeling of the engine is performed with the application of the Least-Squares method and a fourth-order curve fitting to the torque-speed curves provided by the manufacturer for maximum load. The approximation taken is found satisfactory considering the robustness of the proposed SMC scheme to parameter and model uncertainties as well as external disturbances. Using Matlab's polyfit.m function, the engine torque, T_{es} is obtained as a function of engine speed, ω_e as

$$T_{es} = 1.6510^{-7}\omega_e^4 - 0.0002\omega_e^3 + 0.0546\omega_e^2$$
$$- 6.65\omega_e + 361.67$$
$$= \sum_{i=0}^{4} \alpha_i \omega_e^i \tag{1}$$

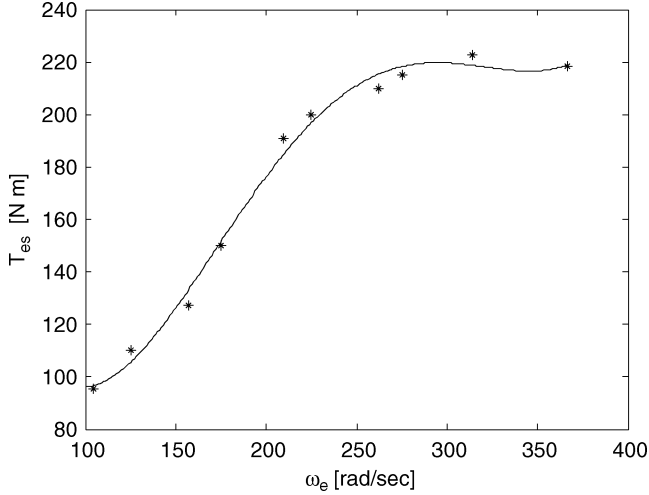Fig. 3. Engine torque speed characteristic.

Fig. 5. Functional block diagram of APU control system.

B. Modeling of the Permanent Magnet Synchronous Generator (PMSG)

The d–q axis model of the permanent magnet synchronous motor (PMSG) is obtained as

$$\frac{di_q}{dt} = -\frac{R}{L_q}i_q + \frac{\omega_e L_d}{L_q}i_d - \frac{1}{L_q}v_q + \frac{K_b}{L_q}\omega_e$$

$$\frac{di_d}{dt} = -\frac{R}{L_d}i_d - \frac{\omega_e L_q}{L_d}i_q - \frac{1}{L_d}v_d$$

$$T_g = K_t i_q + k_1(L_d - L_q)i_d i_q \qquad (3)$$

where

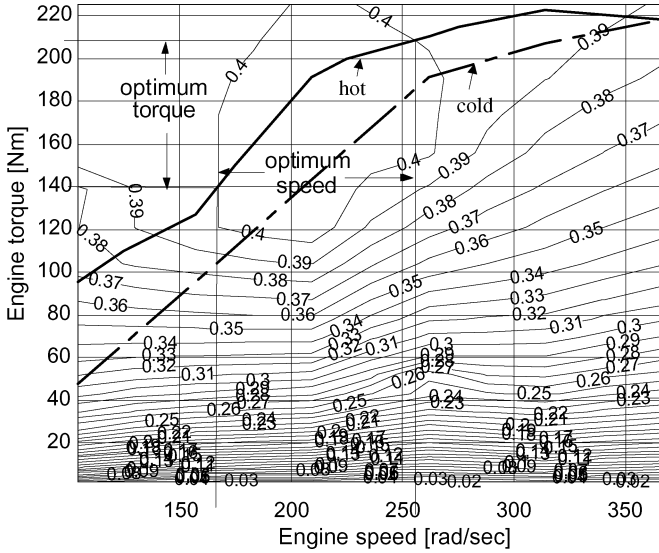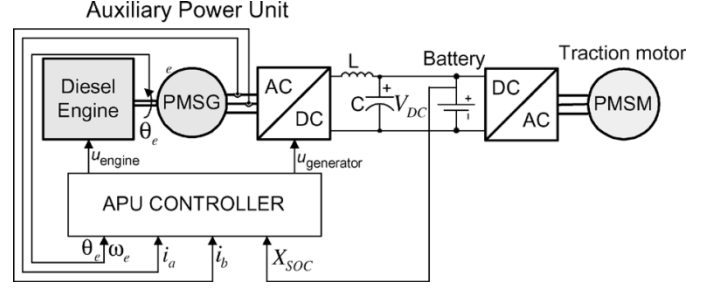|	
i_d, i_q	generator $d - q$ axis currents, respectively;
v_d, v_q	generator $d - q$ axis output voltages, respectively;
R	generator resistance;
L_d, L_q	generator $d - q$ axis inductances, respectively;
K_t	generator torque constant;
K_b	generator induced voltage constant;
T_g	generator torque;
k_1	reluctance torque coefficient;
ω_e	engine speed.

Fig. 4. Engine efficiency map.

where α_i are the polynomial coefficients i $= 0, 1, \ldots, 4$. It is also possible to derive ω_e as a function of T_{es} such as

$$\omega_e = 2.3210^{-6}(T_{es})^4 - 0.001\,14(T_{es})^3 + 0.1937(T_{es})^2$$
$$- 11.839 T_{es} + 267.963$$
$$= \sum_{j=0}^{4} \beta_j T_{es}^j \qquad (2)$$

where β_j are the polynomial coefficients $j = 0, 1, \ldots, 4$.

The engine torque and speed solid line curve obtained from (1) is given in Fig. 3. The points indicated with "$*$" are obtained from the hot engine map provided by the manufacturer.

Using the engine efficiency map, the high efficiency region in Fig. 4, is defined approximately by 140 Nm $\leq$ Tes $\leq$ 210 Nm and 165 rad/s $\leq$ ωe $\leq$ 255 rad/s.

IV. DEVELOPMENT OF THE CONTROL STRATEGY

The control strategy for the APU is based on the following objectives.
— The SOC level will be kept between a given minimum and maximum level.
— The engine will be operated in the optimum efficiency region.

The SOC level of the battery affects the control strategy in the following way.
— When the SOC level evaluated via a hysterisis function decreases to a given minimum level ($SOC_{\min}$), the engine will be started (EC = 1) and stopped when the SOC reaches the given maximum level ($SOC_{\max}$) (EC = 0)

$$EC(t) = \begin{cases} 1, & SOC_{\min} \geq SOC(t) \\ EC(t-1), & SOC_{\max} > SOC(t) > SOC_{\min} \\ 0, & SOC_{\max} \leq SOC(t). \end{cases}$$
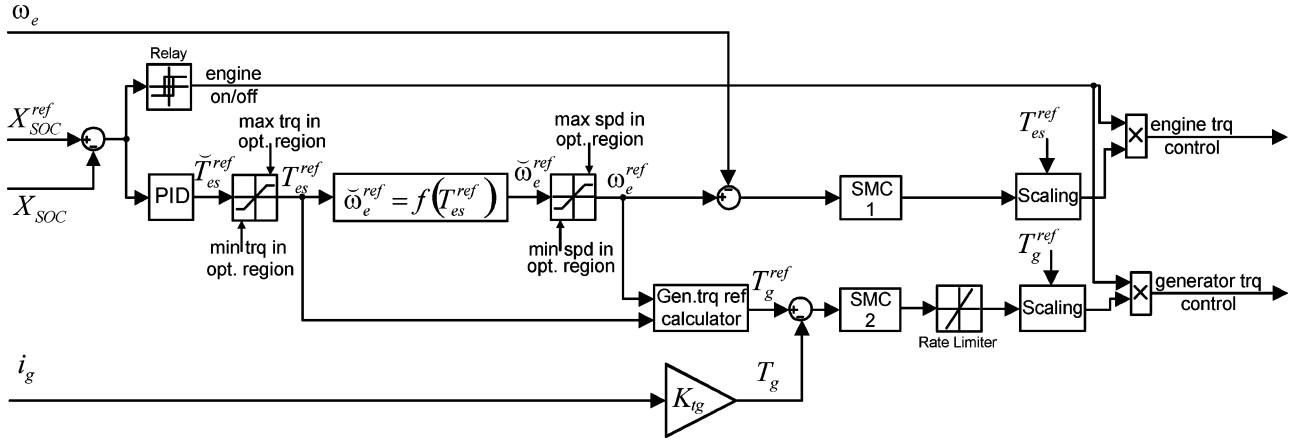
Fig. 6. Detailed block diagram of the APU controller.

— Upon the generation of the start signal, the sliding mode based speed controller (SMC1) and sliding mode based torque controller (SMC2) are run to operate the engine in the optimum efficiency region.

The functional block diagram of the APU control system is given in Fig. 5. The APU controller produces two control signals; -one for the speed control of the engine and the other for the ac/dc converter to control the generator torque using information coming from the battery SOC, generator currents, engine angular velocity and position.

A detailed block diagram for the proposed APU control strategy is also given in Fig. 6. As can be seen in the figure, the APU controller includes two SMCs, one PID, two function blocks—one calculating the engine speed reference and the other for the generator torque reference values, saturation blocks which limit the engine speed and torque reference values to keep the engine operating in the optimal efficiency region, and finally, a relay that produces ON/OFF signals for the APU system.

The APU control system consists of three parts.

A. Linear PID Controller for the Evaluation of SOC

The aim of this controller block is to output the appropriate reference torque value for the engine, taking the error between the reference and actual SOC levels as input. The saturation block placed at the output is to assure that the torque reference stays between the minimum and maximum levels of the optimum efficiency region. Thus, the reference torque is derived from the basic model in (1) for the engine control in the range of $140 \, \text{Nm} \leq T_{es} \leq 210 \, \text{Nm}$, which defines the optimum efficiency region for torque in this case. Using the optimal region for the torque values of the engine and (2), the speed reference for the optimal efficiency region can be given as

$$\omega_e^r = \sum_{j=0}^{4} \beta_j \left(T_{es}^r \right)^j. \tag{4}$$

The calculated speed value is passed through a saturation block to assure a reference speed value within the optimum efficiency region, given as $165 \, \text{rad/s} \leq \omega_e \leq 255 \, \text{rad/s}$.

After the determination of the speed and torque references of the engine control, we will proceed to the design and implementation of the sliding mode based torque and speed control for the

engine. Both controllers are based on the same chattering—free SMC approach and will be derived in the next section for each component.

B. Sliding Mode Based Engine Speed Control

Improvement of the overall efficiency of the SHEV requires efficient control strategies for the diesel engine. However, the engine dynamics are highly nonlinear and cannot be accurately represented with a simple model. Hence, a SMC, which can achieve robustness against structured and unstructured uncertainties of the system is found to be adequate for the aims of the study.

For the control algorithm under consideration, a simple state-space representation must be obtained, also using the engine model derived in (1)

$$\frac{dx_{SOC}}{dt} = Ki_b$$
$$\frac{d\omega_e}{dt} = \frac{1}{J_{tot}} T_{es} - \frac{1}{nJ_{tot}} T_g \tag{5}$$

where

x_{SOC}	state of charge;
i_b	battery current $(i_b = i_q - i_m - i_L)$;
i_m	traction motor currents;
i_L	parasitic electric load current;
i_q	generator quadrature current;
T_g	generator torque;
J_{tot}	total inertia $(J_{tot} = J_g n^2 + J_e)$;
J_e	engine inertia;
J_g	generator inertia;
n	generator speed ratio $= \omega_e/\omega_g = 1.038$

$$K = \frac{1}{3600C_b}$$

C_b battery capacity [Ah].

In (1), the torque function is derived for maximum load; in other words, for maximum throttle level (i.e., 1). However, the throttle level assumes values between 0 and 1 for the control of

the engine. Therefore, the engine torque should be rewritten as a function of the throttle level as follows:

$$T_{es} = u\left(\alpha_0 + \alpha_1\omega_e + \alpha_2\omega_e^2 + \alpha_3\omega_e^3 + \alpha_4\omega_e^4\right) \quad (6)$$

where u is the torque control input (throttle angle 0%–100%).

For $u = 1$, the maximum load torque-speed characteristics are obtained. With the determination of the engine speed reference as above, we now proceed with the development of the SMC, which will produce the optimal throttle angle, u, as output.

First, the polynomial approximation in (1) for T_{es}, is substituted into the following equation of motion for the engine:

$$\frac{d\omega_e}{dt} = \frac{1}{J_{tot}} u \sum_{i=0}^{4} \alpha_i \omega_e^i - \frac{1}{nJ_{tot}} T_g. \quad (7)$$

Next, a sliding surface, σ is chosen as

$$\sigma = \Gamma e \quad (8)$$

where

$$e = \omega_e^r - \omega_e \quad \text{(speed error)}. \quad (9)$$

To ensure the stability of the system, the SMC control law is derived using Lyapunov conditions, similar to the study in [24]. For this purpose, a Lyapunov function, V, is selected as such

$$V = \frac{1}{2}\sigma^2 > 0 \quad (10)$$

$$\dot{V} = \sigma\dot{\sigma} \quad (11)$$

which should be equal to $-D\sigma^2$ to satisfy the negative definiteness of $\dot{V}$. Thus

$$\dot{V} = -D\sigma^2 \quad (12)$$

where $D > 0$.

Consequently

$$\dot{\sigma} + D\sigma = 0. \quad (13)$$

Taking the derivative of σ and substituting the equation of motion inside $\dot{\sigma}$

$$\dot{\sigma} = \Gamma\left(\dot{\omega}_e^r - \dot{\omega}_e\right)$$
$$= \Gamma\dot{\omega}_e^r + \Gamma\frac{1}{nJ_{tot}}T_g - \Gamma\frac{1}{J_{tot}}u\sum_{i=0}^{4}\alpha_i\omega_e^i. \quad (14)$$

Now, an equivalent control input, u_{eq}, that makes $\dot{\sigma} = 0$ will be calculated by replacing u with u_{eq}. This yields

$$u_{eq} = \frac{J_{tot}}{\sum_{i=0}^{4}\alpha_i\omega_e^i}\left(\dot{\omega}_e^r + \frac{1}{nJ_{tot}}T_g\right) \quad (15)$$

$$\dot{\sigma} = \Gamma\frac{1}{J_{tot}}\sum_{i=0}^{4}\alpha_i\omega_e^i(u_{eq} - u). \quad (16)$$

Substituting $\dot{\sigma}$ in (12) into (16) and discretizing this equation together with (16), yields

$$\Gamma\frac{1}{J_{tot}}\sum_{i=0}^{4}\alpha_i\omega^i(k)\left(u_{eq}(k) - u(k)\right) + D\sigma(k) = 0 \quad (17)$$

and

$$\frac{\sigma(k) - \sigma(k-1)}{T} = \Gamma\frac{1}{J_{tot}}$$
$$\times \sum_{i=0}^{4}\left[\alpha_i\omega^i(k-1)\left(u_{eq}(k-1) - u(k-1)\right)\right]. \quad (18)$$

With the assumption that equivalent control is an average value

$$u_{eq}(k) \approx u_{eq}(k-1). \quad (19)$$

This yields a chattering-free sliding mode (SM) of the following form:

$$u(k) = u(k-1) + \frac{J_{tot}}{\Gamma T\sum_{i=0}^{4}\alpha_i\omega_e^i(k)}\left((1 + DT)\sigma(k) - \sigma(k-1)\right) \quad (20)$$

where Γ, D are positive design parameters.

C. Sliding Mode Based Generator/Engine Torque Control

At this stage, the reference torque value for the generator is calculated as below, utilizing the optimum reference torque value of the engine derived using the PID controller, optimal reference value of the engine speed and the total inertia of the APU

$$T_g^r = T_{es}^r - J_{tot}\dot{\omega}^r. \quad (21)$$

A chattering-free sliding mode torque controller is designed based on the permanent magnet ac generator model in (2), which is organized in state-space form as

$$\frac{d}{dt}\underbrace{\begin{bmatrix} i_d \\ i_q \end{bmatrix}}_{x_g} = \underbrace{\begin{bmatrix} -\frac{R}{L_d} & 0 \\ 0 & -\frac{R}{L_d} \end{bmatrix}}_{A_g}\begin{bmatrix} i_d \\ i_q \end{bmatrix} + \underbrace{\begin{bmatrix} \frac{L_d}{L_q}\omega_e i_d + \frac{K_b}{L_q}\omega_e \\ \frac{L_q}{L_d}\omega_e i_q \end{bmatrix}}_{\eta}$$
$$+ \underbrace{\begin{bmatrix} -\frac{1}{L_d} & 0 \\ 0 & -\frac{1}{L_d} \end{bmatrix}}_{B_g}\underbrace{\begin{bmatrix} v_d \\ v_q \end{bmatrix}}_{u_g}$$
$$T_g = K_t i_q + K_1(L_d - L_q)i_d i_q. \quad (22)$$

Because the number of rotor teeth is high enough, it can be assumed that $L_d \approx L_q$ and the generator torque is

$$T_g \approx K_t i_q. \quad (23)$$

In state space form

$$\dot{x}_g = A_g x_g + B_g u_g + \eta$$
$$y = T_g = \begin{bmatrix} 0 & K_t \end{bmatrix} \begin{bmatrix} i_d \\ i_q \end{bmatrix}. \quad (24)$$

By forcing the generator current d-axis component, i_d, to be zero, the torque control can be achieved via the q-axis component of the generator current, i_q.

The sliding surface should thus be chosen as:

$$\sigma_g = \begin{bmatrix} e_d \\ e_q \end{bmatrix} = \begin{bmatrix} i_d^r - i_d \\ i_q^r - i_q \end{bmatrix}. \quad (25)$$

The i_d^r is taken as zero to make $i_d = 0$. The q-axis current component reference value is then calculated using the reference torque value of the generator

$$i_q^r = \frac{T_g^r}{K_t}. \quad (26)$$

Once again, the candidate Lyapunov function is chosen as

$$V_g = \frac{1}{2} \sigma_g^T \sigma_g; \quad \dot{V}_g = \sigma_g^T \dot{\sigma}_g = -\sigma_g^T D_g \sigma_g. \quad (27)$$

The strictly positive matrix, D_g is

$$D_g = \begin{bmatrix} d_1 & 0 \\ 0 & d_2 \end{bmatrix}; \quad d_1, d_2 > 0 \quad (28)$$

such that

$$\dot{\sigma}_g = -D_g \sigma_g \quad (29)$$
$$\dot{\sigma}_g = \dot{x}_g^r - \dot{x}_g = \dot{x}_g^r - A_g x_g - B_g u_g - \eta. \quad (30)$$

The equivalent control can be derived using the same idea as in (11)

$$u_{g\_eq} = B_g^{-1} \left(\dot{x}_g^r - A_g x_g - \eta \right). \quad (31)$$

Using the similar approach taken as in (12)–(17), the control law can be derived as

$$u_g(k) = u_g(k-1) + \frac{B_g^{-1}}{T} \left[(I + D_g T)\sigma_g(k) - \sigma_g(k-1) \right] \quad (32)$$

where

$$u_g = \begin{bmatrix} v_d^r \\ v_q^r \end{bmatrix}.$$

Fig. 7 represents the control mechanism of generator torque.

V. SIMULATION RESULTS

The developed control methods in this study are tested on a computer simulation model of the XM1124 prototype created using the Matlab/Simulink based PNGV Systems Analysis Toolkit (PSAT Version 4.1) [22]. PSAT is a forward-looking vehicle modeler. The vehicle model is created using component
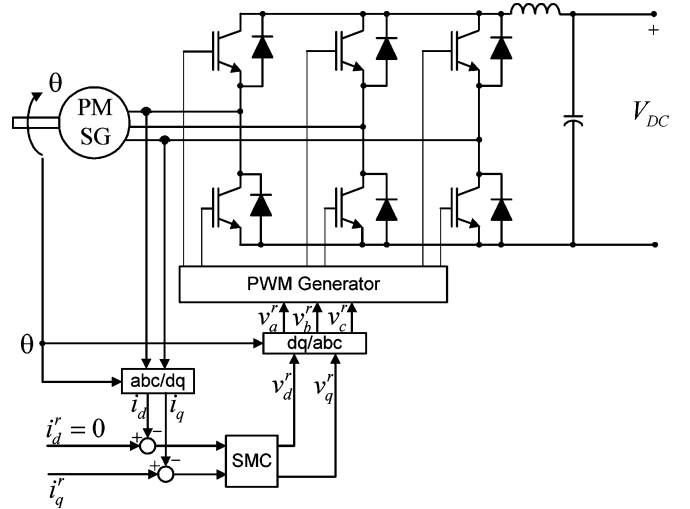

Fig. 7. Detailed block diagram of generator torque control.

modules for various vehicle systems. PSAT ties these modules together into a complete vehicle model which it drives in accordance with various drive cycle scenarios specified by the user. Since this PSAT model was created while the prototype was being manufactured, the individual component modules were based on parameters provided by vendors of the vehicle components or were standard components which are provided in the basic PSAT libraries.

In the initial stage of our studies, performance predictions based on PSAT models for engine/fuel utilization, battery energy utilization, and traction power required were compared to performance data measured during field testing of the prototype HMMWV [23]. Comparison of the actual performance with the simulation results indicated that the simulation model needed only minor modifications to reflect actual vehicle parameters versus those specified by the vendors and the correlation between the model's predictions and the test data showed that the model could be used as a baseline upon which alternate components, configurations, and control strategies can be built and evaluated.

The performance of the SMC based control strategy was tested using a drive cycle simulation. The Federal Urban Drive Cycle (FUDS) with a total duration of 1,371 s and traveled distance of 12 km is used for this purpose. The FUDS emulates the type of driving expected in an urban environment with many accelerations and decelerations at moderate speeds. While this may not be the typical drive cycle for a military HMMWV, it does offer a well recognized standard for comparison. At this time, there is no standard drive cycle which represents the mission driving requirements for a military HMMWV. Therefore, the FUDS cycle will be taken into consideration, as it offers the advantage of dictating the type of stop-and-go driving, with its associated power demand cycling required to tax the capabilities of a HEV.

In this study, for a realistic performance evaluation of the developed SMC based control strategies, three sets of simulations are performed—one using the original strategies offered by the standard PSAT model; another utilizing the SMC based engine control only, while employing the generator control strategy of-
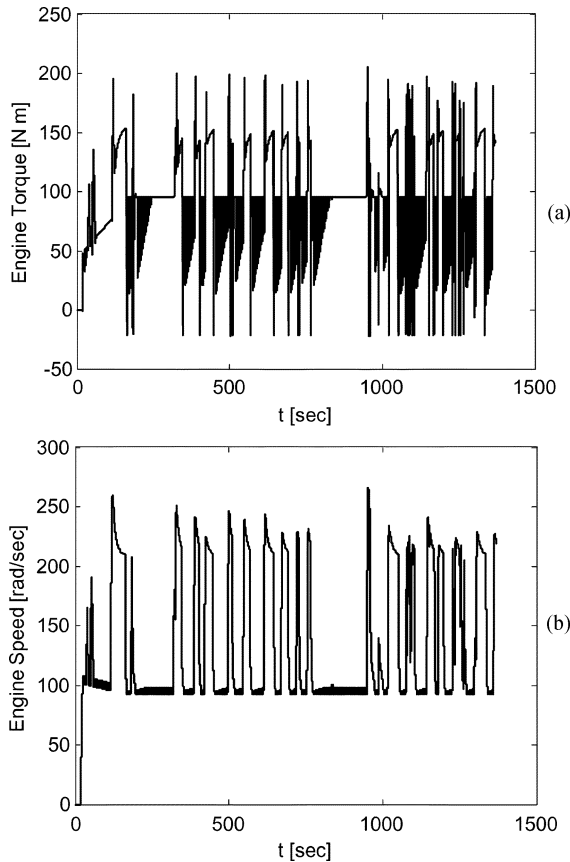
Fig. 8.   (a) Engine torque and (b) engine speed (original PSAT).

Fig. 9.   Traction motor: (a) torque and (b) speed variations.

fered by the standard PSAT model and finally, the new SMC based strategy, controlling the engine speed and engine/generator torque. The traction motor control strategy is kept the same for all three approaches and therefore, its performance will be demonstrated for the PSAT model only.

The original PSAT strategies are based on logical decision blocks that use PI based controllers with an additional feedforward term (scaled torque demand value due to the engine map) as well as engine, generator, and power converter maps. The simulation results obtained with this prototype control strategy are given in Fig. 8(a) and (b) depicting the engine torque and speed, while Fig. 9(a) and (b) give the traction motor torque and speed with the same approach. The traction motor outputs track the FUDS cycle quite closely; however, inspecting the results further, it can easily be observed that the engine is always on and goes into idle mode during battery only operation. This presents a major disadvantage of this strategy, since in the idle mode, the efficiency of the engine is very poor.

One of the major aims of the proposed control strategy is to remedy this issue by not allowing the engine to operate outside of its optimal efficiency region, except for short transients. This is achieved by controlling the engine speed and torque using SMC, which also ensures robustness against parameter and model uncertainties of the engine and generator. To further emphasize the improvement made with the developed SMCs for both engine speed and torque control, simulation results are also obtained for the case which uses the new SMC for the engine speed control only, while utilizing the generator control offered by PSAT based on maps and PI controllers.
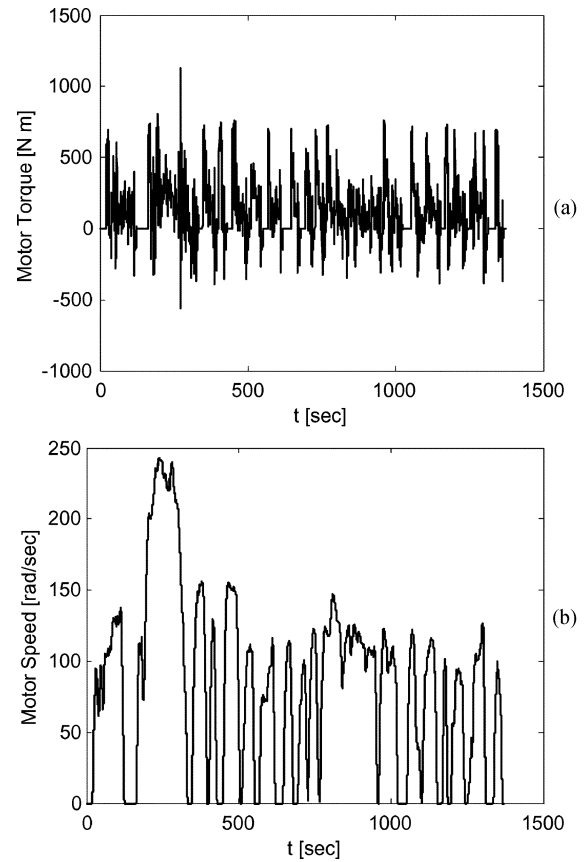
The reference and actual torque and speed variations for this case are given in Fig. 10(a) and (b), while Fig. 11(a) and (b) depict torque and speed variations for the new control strategy, which uses a SMC based algorithm for the engine/generator torque as well. For ease of description in the figures, the engine speed control scheme based on one SMC only is denoted as 1-SMC, while the new scheme based on two SMCs is labeled 2-SMC. Inspecting all four outputs, it can easily be observed that a much better reference tracking performance is obtained with the strategy based on 2-SMC. Also, the engine off durations are observed to occur during battery utilization only, as well as the effect of the generator torque rate limiter in the torque outputs in both cases, which has been added to the system to provide a mild transient for the engine.

Next, the SOC variations for all three strategies are given in Fig. 12. As can be seen in the figure, the sliding mode based control strategies, 1-SMC and 2-SMC, allow larger variations in the SOC. This is a result of the fact that the SMC based strategies operate the engine only in the high efficiency region and when the engine is off, all power is drawn from the batteries. However, in spite of these larger fluctuations, the SMC based strategies result in higher final SOC values in comparison to the original PSAT results. An even higher final level is achieved with the 2-SMC based strategy due to a more efficient use of the engine with the designed generator torque control.

Fig. 13(a)–(c) depict the efficiency diagrams of the engine for the strategies offered by the original PSAT, 1-SMC, and 2-SMC, respectively. Both SMC algorithms based on operating the engine only in its high efficiency region yield improved engine
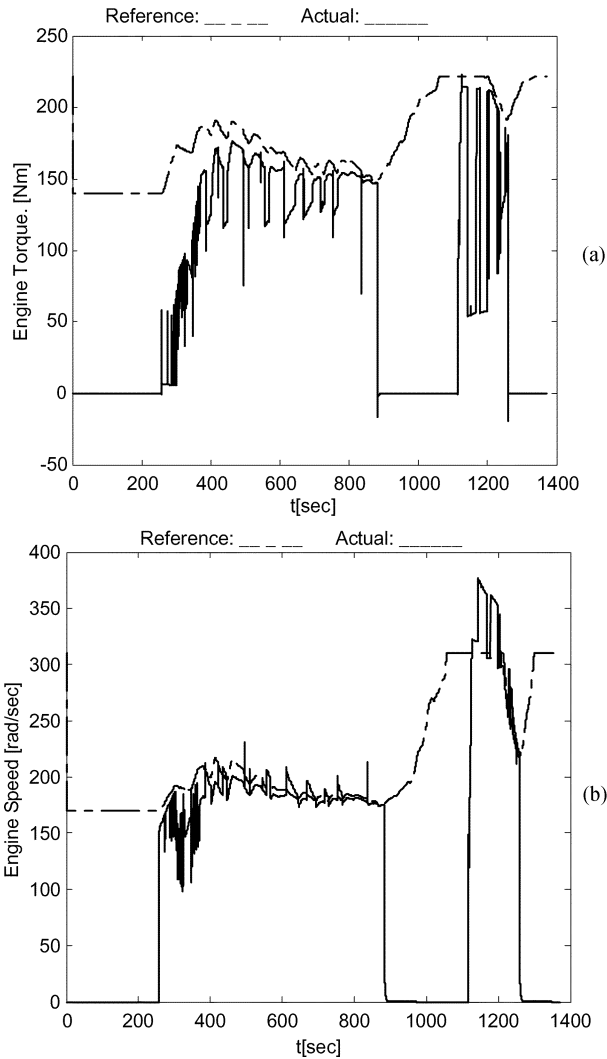
Fig. 10. Reference and actual variations: (a) torque and (b) speed with 1-SMC.

Fig. 11. Reference and actual variations: (a) torque and (b) speed with 2-SMC.

Fig. 12. SOC levels for the three strategies.

efficiency, as opposed to the strategy used in the PSAT, which keeps the engine on at all times. Efficiency is even more improved with the addition of the generator torque control, as can be seen in Fig. 13(c). The efficiency map in Fig. 13 includes all engine speed and torque values obtained during the whole operation cycle. Thus, operation points appearing outside of the high efficiency region relate to engine transients, which in fact, occur less frequently.

Finally, the simulation results for all three approaches are tabulated in Table I. The mileage, efficiency, and emissions values for all strategies are derived based on calculations utilized in PSAT [22], i.e., the overall efficiency is the ratio of the total propulsive energy to the energy supplied by the fuel corrected for SOC changes from drive cycle start to stop; the engine efficiency on the other hand, is calculated separately during acceleration and deceleration modes as the ratio of the shaft energy output to the fuel energy input. Inspection of the result for each performance criterion indicates the improvement made with the new strategy in terms of overall system efficiency, engine efficiency, fuel economy, final SOC level, and emissions. The expressions used for the calculation of the performance criteria in Table I, are listed in the Appendix.
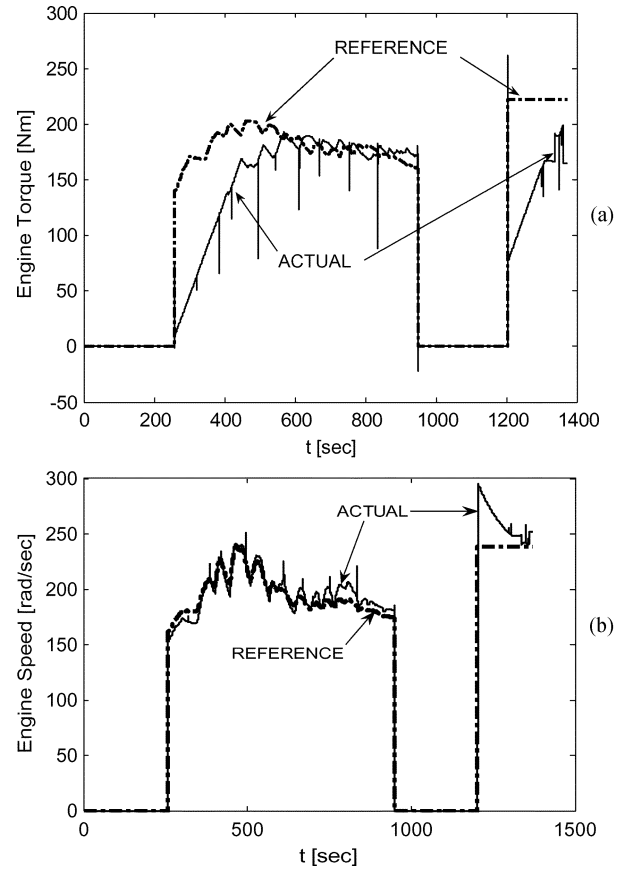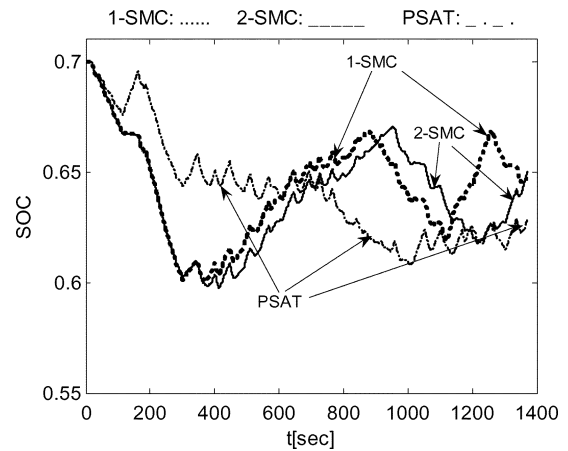
VI. CONCLUSION

In this study, the optimized operation of the internal combustion engine is aimed to improve the overall efficiency of a SHEV. As a novel approach in the control of SHEVs, two chattering-free SMCs are developed to keep the engine operation in the optimal efficiency region, whenever the engine operation is required due to a drop in the SOC level. One of the SMCs is dedicated for engine speed control, while the other performs engine/generator torque control via the power converter. Due to the robustness properties offered by the SMCs, only a simple
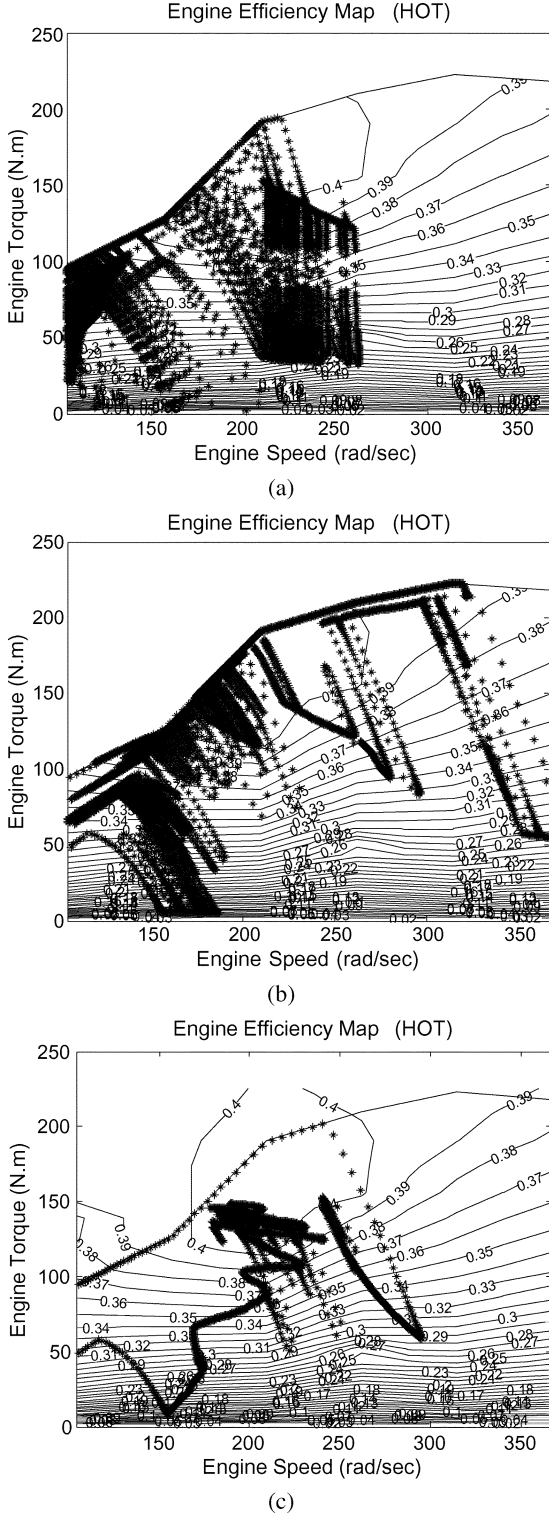
Fig. 13.   Engine efficiency diagrams: (a) with original PSAT, (b) with 1-SMC, and (c) with 2-SMC.

model is required for each APU component; namely, the engine, generator and power converter.

To highlight the benefits of the new control strategy based on two SMCs (2-SMC), the performance of the control system is compared with that obtained with the original PSAT strategy, which utilizes comprehensive cold and hot engine maps (static

TABLE I
PERFORMANCE TABLE FOR THE TWO STRATEGIES

	Original PSAT	1-SMC	2-SMC
Overall Efficiency	21.98 %	22.303 %	22.45 %
Average Engine Efficiency	0.39 (acc.)-0.36 (dec.)	0.39-0.37	0.39 – 0.39
MPG	16.15	16.39	16.495
Ending SOC	0.646	0.647	0.650
HC emission (g/mil)	1.0957	0.936	1.077
CO emission (g/mil)	5.513	1.867	3.106
CO_2 emission (g/mil)	547.68	545.95	539.95
Fuel mass (kg)	1.309	1.288	1.279

only), PI controllers and a feedforward term for the engine torque. To emphasize further the benefits of the designed engine/generator torque control, the performance of the 2-SMC is also compared with a strategy aiming to keep the engine in its high efficiency region by a SMC based engine control only (1-SMC), while generator torque control is performed using the original PSAT strategies.

The SMC based strategies both demonstrate the expected robustness with their tracking performance of the speed and torque references in the optimal efficiency region, despite load variations, which can be observed from traction motor curves. The addition of the generator torque control in the 2- SMC strategy yields an even more improved performance in terms of overall efficiency, engine efficiency, fuel economy and emissions in spite of the simple approach taken to model the APU and the optimal efficiency region of the engine. The proposed SMC based scheme also offers additional benefits such as modularity and ease of application to other SHEV systems with model and parameter uncertainties.

APPENDIX

Overall Efficiency:

$$\eta = 100 \frac{\int_0^{t_{\text{end}}} F_v(t)v(t)dt + E_{b\_out\_acc}}{\int_0^{t_{\text{end}}} H_v m_f(t)dt + E_{b\_in\_acc}}$$

where v is the vehicle speed, H_v is the heating value of fuel, m_f is the mass flow rate of fuel, and $F_v = T_{tc} - T_{br}/r_{wh}$ is the vehicle affected force.

Here, $T_{tc} = (T_{m1} + T_{m2})\eta_{tc}\alpha_{tc}$ is the transfer case torque, T_{br} is brake torque, T_{m1}, T_{m2} are the motor torques; η_{tc} α_{tc} are the transfer case efficiency and gear ratio, respectively; r_{wh} is the wheel radius; $E_{b\_in\_acc} = \sum i_b(t_{acc})v_{OC}(t_{acc})t_{acc}$, and $E_{b\_out\_acc} = \sum i_b(t_{acc})v_b(t_{acc})t_{acc}$ are the battery input and output energy in acceleration.

Here, $t_{acc} = t|_{\substack{v \neq 0 \\ T_{dr}^{ref} \geq 0}}$, $t_{dec} = t|_{\substack{v \neq 0 \\ T_{dr}^{ref} < 0}}$ are the acceleration and deceleration times, respectively; and $i_b(t_{acc})$, $v_{OC}(t_{acc})$,

$v_b(t_{\text{acc}})$ are the battery current, open circuit voltage and voltage in acceleration.

Engine Efficiency: Here, $\eta_{\text{acc}} = E_{\text{out\_acc}}/E_{\text{in\_acc}}$, $\eta_{\text{dec}} = E_{\text{out\_dec}}/E_{\text{in\_dec}}$ are the engine efficiency at acceleration and deceleration; where $E_{\text{in\_acc}} = \sum H_v m_f(t_{\text{acc}})t_{\text{acc}}/\sum t_{\text{acc}}$, $E_{\text{out\_acc}} = \sum T_e(t_{\text{acc}})\omega_e(t_{\text{acc}})t_{\text{acc}}/\sum t_{\text{acc}}$ are the engine input and output energy in acceleration; and $E_{\text{in\_dec}} = \sum H_v m_f(t_{\text{dec}})t_{\text{dec}}/\sum t_{\text{dec}}$, $E_{\text{out\_dec}} = \sum T_e(t_{\text{dec}})\omega_e(t_{\text{dec}})t_{\text{dec}}/\sum t_{\text{dec}}$ are the engine input and output energy in deceleration; where T_e and ω_e are the engine torque and angular speed.

MPG (Fuel Economy):

$$\text{fuel\_economy} = \frac{\int\limits_0^{t_{\text{end}}} v(t)dt}{\int\limits_0^{t_{\text{end}}} m_f(t)dt}.$$

Ending SOC:

$$\text{SOC}(t) = \frac{C_{\text{max\_}b}(\theta_b) - \frac{1}{3600}\int i_b dt}{C_{\text{max\_}b}(\theta_b)}$$

where $C_{\text{max\_}b}(\theta_b)$ is the maximum battery capacity by function of the battery temperature (A-h)

$$\text{SOC}(t_{\text{end}}): \text{ final SOC value}(\text{t} = 1372\text{ x}).$$

Emission:

  a) CO emission:

$$e_{CO} = \text{Table}_{\text{CO\_conversion\_efficiency}}(\theta_{\text{cat}}, m_f)\eta_{\text{cat}}r_{CO}$$

where η_{cat} is the catalyst efficiency; $r_{CO} = m_f \times \text{Table}_{\text{CO\_emission\_index}}(T_e, \omega_e)$ is the CO rate; and $\theta_{\text{cat}} = (1/\tau_{ex\_hot})\int r_{ex\_hot} \times (\theta_{ex\_hot} - \theta_{\text{cat}})dt + (1/\tau_{ex\_cold})\int [1 - r_{ex\_cold} \times (\theta_{ex\_hot} - \theta_{\text{cat}})]dt$ is the catalyst temperature.

Here, $r_{ex\_hot} = \text{Table}_{ex\_hot}(T_e, \omega_e)$ is the exhaust rate; θ_{ex_hot} is the hot catalyst temperature; and $\tau_{ex\_hot}, \tau_{ex\_cold}$ are the exhaust hot and cold time constants, respectively.

  b) CO2 emission:

$$e_{CO2} = \frac{44}{12}\left[m_f r_{\text{fuel\_carbon}} - \frac{12}{28}e_{CO} - e_{HC}r_{\text{fuel\_carbon}}\right]$$

where r_{fuel_carbon} is the fuel-carbon ratio; and $e_{HC} = \text{Table}_{\text{HC\_conversion\_efficiency}}(\theta_{\text{cat}}, m_f)\eta_{\text{cat}}r_{HC}$ is the HC emission value; where $r_{HC} = m_f \times \text{Table}_{\text{HC\_emission\_index}}(T_e, \omega_e)$ is the HC rate.

REFERENCES

[1] M. Ehsani, Y. Gao, S. E. Gay, and A. Emadi, *Modern Electric, Hybrid Electric, and Fuel Cell Vehicles—Fundamentals, Theory, and Design*. Boca Raton, FL: CRC, 2005.

[2] C. C. Chan and K. T. Chau, *Modern Electric Vehicle Technology*. Oxford, U.K.: Oxford University Press, 2001.

[3] A. Emadi, M. Ehsani, and J. M. Miller, *Vehicular Electric Power Systems—Land, Air, And Space Vehicles*. New York: Marcel Dekker, Inc., 2004.

[4] C. C. Chan and Y. S. Wong, "Electric vehicles charge forward," *IEEE Power Energy Mag.*, vol. 2, no. 6, pp. 24–33, Nov./Dec. 2004.

[5] A. Emadi, *Handbook of Automotive Power Electronics and Motor Drives*. Boca Raton, FL: CRC, 2005.

[6] S. Onoda and A. Emadi, "PSIM-based modeling of automotive power systems: conventional, electric, and hybrid electric vehicles," *IEEE Trans. Veh. Technol.*, vol. 53, no. 2, pp. 390–400, Mar. 2004.

[7] B. K. Powell, K. E. Bailey, and S. R. Cikanek, "Dynamic modeling and control of hybrid electric vehicle powertrain systems," *IEEE Control Syst. Mag.*, vol. 18, no. 5, pp. 17–33, Oct. 1998.

[8] R. Saeks, C. J. Cox, J. Neidhoefer, P. R. Mays, and J. J. Murrey, "Adaptive control of a hybrid electric vehicle," *IEEE Trans. Intell. Transport. Syst.*, vol. 3, no. 4, pp. 213–234, Dec. 2002.

[9] G. Fiengo, C. Di Fiore, D. Lepore, and F. Vasca, "Auxiliary power unit control for hybrid electric vehicle," in *Proc. Eur. Control Conf.*, Cambridge, U.K., 2003, pp. 2339–2344.

[10] S. Onada and A. Emadi, "PSIM-based modeling of automotive power systems: conventional, electric, and hybrid electric vehicles," *IEEE Trans. Veh. Technol.*, vol. 53, no. 2, pp. 390–400, Mar. 2004.

[11] S. Barsali, C. Miulli, and A. Posenti, "A control strategy to minimize fuel consumption of series hybrid electric vehicle," *IEEE Trans. Energy Conv.*, vol. 19, no. 1, pp. 187–195, Mar. 2004.

[12] X. He and J. W. Hodgs, "Modeling and simulation for hybrid electric vehicles—part I: modeling," *IEEE Trans. Intell. Transport. Syst.*, vol. 3, no. 4, pp. 235–243, Dec. 2002.

[13] X. He and J. W. Hodgson, "Modeling and simulation for hybrid electric vehicles—part II: simulation," *IEEE Trans. Intell. Transport. Syst.*, vol. 3, no. 4, pp. 244–251, Dec. 2002.

[14] S. Barsali, M. Ceraolo, and A. Posenti, "Techniques the control the electricity generation in a series hybrid electric vehicle," *IEEE Trans. Energy Conv.*, vol. 17, no. 2, pp. 260–266, Jun. 2002.

[15] K. D. Young, V. I. Utkin, and U. Ozguner, "A control engineer's guide to sliding mode control," *IEEE Trans. Contr. Syst. Technol.*, vol. 7, no. 3, pp. 328–342, May 1999.

[16] V. Utkin, H.-C. Chang, I. Kolmanovsky, and J. Cook, "Sliding mode control for variable geometry turbocharged diesel engines," in *Proc. Amer. Contr. Conf.*, 2000, pp. 584–588.

[17] K. B. Goh, S. K. Spurgeon, and B. Jones, "Higher-order sliding mode control of a diesel generator set," in *Proc. Inst. Mech. Eng. (IMechE), Part I: Syst. Contr. Eng.*, 2003, pp. 229–241.

[18] I. Haskara, C. Hatipoglu, and U. Ozguner, "Sliding mode compensation, estimation and optimization methods in automotive control problems," in *Variable Structure Systems: Towards the 21st Century*. New York: Springer–Verlag, 2002, pp. 155–174.

[19] I. Bhatti, S. K. Spurgeon, R. Dorey, and C. Edwards, "Sliding mode configurations for automotive engine control," *Int. J. Adaptive Contr. Signal Process.*, vol. 13, pp. 49–60, 1999.

[20] M. Gokasan, S. Bogosyan, E. Bargar, and D. Goering, "Improved Powertrain Control of an HE-HMMWV," presented at the Annual Society of Automotive Engineers (SAE) Conference, 2005.

[21] S. Fish, T. Savoie, and H. Vanicek, "Modeling hybrid electric HMMWV power system performance," *IEEE Trans. Magn.*, vol. 37, no. 1, pp. 480–484, Jan. 2001.

[22] A. Rousseau, *PSAT V4.1 User's Manual*. Chicago, IL: Argonne National Laboratory, 2001.

[23] H. E. Bargar, J. Li, D. Goering, and J. Lee, "Modeling and verification of hybrid electric HMMWV performance," in *Proc. IEEE IECON*, 2003, pp. 939–944.

[24] O. S. Bogosyan, M. Gokasan, and A. Sabanovic, "A sliding mode based disturbance observer for motion control systems," in *Proc. VSS'99 Conf.*, 1999, pp. 91–95.
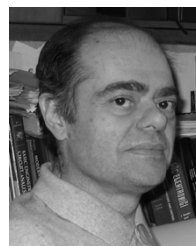
Metin Gokasan (M'95) received the B.Sc., M.Sc., and Ph.D. degrees in electrical and control engineering from Istanbul Technical University (ITU), Istanbul, Turkey, in 1980, 1982, and 1990, respectively.

He is an Associate Professor at the Electrical and Electronics Engineering Department, ITU, and is currently a Visiting Professor at the University of Alaska, Fairbanks. His research interests are control of electrical machinery, power electronics, control of hybrid electric vehicles, and mechatronics systems.

Dr. Gokasan is a member of the Technical Committee on Education in Engineering and Industrial Technologies, IEEE Industrial Engineering Society.

Seta Bogosyan (M'95–SM'05) received the B.S., M.S., and Ph.D. degrees in electrical and control engineering from Istanbul Technical University (ITU), Istanbul, Turkey, in 1981, 1983, and 1991, respectively.

She conducted her Ph.D. studies at the Center for Robotics, University of California at Santa Barbara, where she was a research scientist and lecturer from 1987 to 1991. For the last decade, she has worked as an Associate Professor at ITU and is currently a faculty member with the Electrical and Computer Engineering Department, University of Alaska, Fairbanks. Her fields of interest are robot and motion control, remote robotics and mechatronics laboratories, data fusion with multisensor networks, and applications of nonlinear control to electromechanical systems.

Dr. Bogosyan is currently Vice President of Membership of the IEEE Industrial Engineering Society, as well as Chair of the Technical Committee on Education in Engineering and Industrial Technologies.

Douglas J. Goering received the B.S. degrees in physics and mechanical engineering from the University of Washington, Seattle, in 1981, the M.S. degree in mechanical engineering from the University of Alaska, Fairbanks, in 1984, and the Ph.D. degree in mechanical engineering from the University of California, Berkeley, in 1989.

He is currently a Professor and Chair with the Mechanical Engineering Department, University of Alaska, Fairbanks. He has over 20 years of research experience including an extensive background in computer modeling and simulation. His primary research interests are in the areas of heat transfer, fluid mechanics, energy systems, automotive power plants, and hybrid vehicles. He has worked extensively in the areas of computational heat transfer and fluid mechanics and has more recently been devoting his attention to research involving automotive technology. He currently serves as Principal Investigator or Co-Principal Investigator on several projects that are aimed at the investigation of hybrid vehicles with particular emphasis on their performance in extreme environments.